Journal of Intelligent & Robotic Systems (2025) 111:67
https://doi.org/10.1007/s10846-025-02277-6

REGULAR PAPER

A Multi-UAV Approach for Fast Inspection of Overhead Power Lines: From Route Planning to Field Operation

Alvaro Caballero[1] · Francisco Javier Roman-Escorza[1] · Ivan Maza[1] · Anibal Ollero[1]

Received: 30 November 2024 / Accepted: 20 May 2025 / Published online: 31 May 2025
© The Author(s) 2025

Abstract
Overhead power lines are critical infrastructures to ensure a reliable energy supply, and failures in the grid can lead to significant service disruptions. Locating these faults quickly is crucial but often challenging, especially in hard-to-reach areas such as mountainous regions. This paper presents an integrated solution for the long-range visual inspection of overhead power lines in minimum time using teams of Unmanned Aerial Vehicles (UAVs). The solution, designed for effective field operation while meeting end-user requirements, comprises route planning, autonomous execution, and monitoring of the inspection mission. Concerning route planning, a capacitated min-max multi-depot vehicle routing problem has been formulated to compute feasible routes that cover the entire grid in minimum mission time. The method can be applied to heterogeneous multi-UAV teams in terms of inspection speed and battery consumption, which helps maximise the utilisation of available robots. Moreover, the planning method is complemented by an accurate battery-consumption model based on energy principles that captures the effect of parameters often overlooked such as UAV mass, inspection speed, and weather conditions. The model has shown estimates with relative errors not exceeding 1.34% compared to real measurements. The proposed solution has been experimentally validated under real-world conditions, enabling the autonomous multi-UAV inspection of more than 10 kilometres of real power lines in 13 minutes, which represents a time reduction of up to 67.21% compared to the state of the art. The resulting videos enabled the identification of a simulated power outage and its exact location.

Keywords Unmanned aerial vehicles · Aerial robotics · Inspection · Path planning

1 Introduction

Power transmission lines are crucial assets for our society. Stretching over thousands of kilometers, power grids deliver electricity nationwide to millions of people, enabling critical industrial activities, supporting vital services, and contributing significantly to the economic stability of any region. To maintain the reliability of electricity supply, utility companies allocate substantial financial resources to both building the infrastructure and implementing robust Inspection and Maintenance (I&M) strategies to prevent potential disruptions in the service and the related costs [1].

Over the past few years, the use of UAVs (Unmanned Aerial Vehicles) in I&M tasks for overhead power lines has attracted increasing attention. There are commercial solutions such as [2] that aim to prevent human operators from working at height, greatly enhancing operational safety while decreasing costs. From a research perspective, the H2020 AERIAL-CORE project[1] has played a pivotal role in advancing the field. This project addressed a broad range of I&M operations in overhead power lines, which can be classified into long-distance inspection, aerial manipulation, and aerial co-working. These tasks encompass accurate 3D mapping of power lines [3], autonomous power-grid inspections using advanced control techniques [4], deploying bird-flight diverters, sensors, and other equipment via aerial robotic manipulators [5–7], as well as enabling interactions between

✉ Alvaro Caballero
alvarocaballero@us.es

Francisco Javier Roman-Escorza
froman2@us.es

Ivan Maza
imaza@us.es

Anibal Ollero
aollero@us.es

[1] GRVC Robotics Lab, University of Seville, Camino de los Descubrimientos S/N, Seville 41092, Spain

[1] https://aerial-core.eu/

aerial robots and humans working at height for tool handover [8], among other activities. Parallel research initiatives also propose aligned developments [9–11].

While numerous specific challenges associated with using UAVs for I&M tasks on overhead power lines have been addressed in the literature, most studies concentrate on two primary approaches: precise inspection of individual transmission towers and long-range inspection of entire power grids. In both scenarios, planning techniques are crucial to achieve useful outcomes [12–18].

For the precise inspection of individual transmission towers, the planning approach typically involves combining various inspection goals into an optimisation problem to compute a path that remains inside a restricted workspace. A notable example is presented in [12], where an optimisation problem is formulated by considering flight time, image quality, and tower coverage. This problem is addressed using particle swarm optimisation and simulated annealing, achieving a well-balanced trade-off among these three performance metrics. Some studies incorporate multiple UAVs to accelerate the inspection process. However, this increases the complexity of planning, as safety between UAVs must be guaranteed throughout the mission. Signal Temporal Logic can be applied to ensure this safety requirement is met, along with the other objectives [13].

In contrast, the planning problem for long-range power-grid inspection typically comprises flying large distances while optimising routes and adhering to coverage requirements and battery limitations. Given that the VRP (Vehicle Routing Problem) and its variations have proven effectiveness for planning tasks modelled as graphs [19], most state-of-the-art approaches for power grid inspection treat the planning problem as a variant of this method. In this context, [14] proposes a generalisation of the TSP (Traveling Salesman Problem) for efficient UAV-based transmission-line inspections. The formulation accounts for the limited flight time of UAVs and introduces multi-tour strategies to ensure full coverage of the power grid. However, the solution focuses on the use of single UAVs, which may prove inadequate for practical applications due to their limited endurance. To address this, other publications explore the coordinated use of UAVs with ground vehicles that deploy and recover them for extended range operations [15–17], or consider multi-UAV strategies that inspect all the electric towers inside a designated area but overlook the connecting cables [18]. There are also contributions proposing the use of multi-robot networks for general monitoring and inspection operations, which can be adapted to power-grid inspection [20].

Despite the valuable publications on route planning for long-range inspection of power grids, most of these contributions prioritise the formulation of theoretical problems and their solution methods without thoroughly evaluating the effectiveness of the resulting plans during real-world UAV inspections. Thus, many of them focus on solving large grids, sometimes artificially complex, in bounded computation times. However, they are at the same time disregarding practical aspects like current regulatory constraints, the effect of weather conditions in the planned routes or requirements imposed by end users to guarantee certain quality level in the captured images or videos. In addition, they usually assume the availability of information that is sometimes not easily accessible in practice, such as the accurate location of electric towers. To the best of the authors' knowledge, there are no prior publications devoted to the autonomous long-range inspection of overhead power lines using a multi-UAV team with effective operation in real field experiments.

1.1 Contributions and Outline

This article is an extension of the conference paper [21]. In that publication, a route planning method for fast inspection of overhead power grids using a team of UAVs was first presented and analysed, and preliminary experiments were carried out as a first proof of concept. The method, which incorporates battery constraints and supports heterogeneous UAVs in terms of flight speed and battery capacity, can integrate a clustering approach to reduce computational load while preserving the quality of the solution.

This article builds upon the previous route planner and enhances it by adding several new features. The result is an integrated solution that allows a multi-UAV team to autonomously perform the effective long-range inspection of overhead power grids in real-world conditions (see Fig. 1), producing useful videos as the output. More in detail, the main contributions of this paper can be enumerated as follows:

Fig. 1 Multi-rotor aerial robot autonomously executing a long-range multi-UAV mission for visual inspection of a real overhead power line

1. Adaptation of the inspection approach presented in [21] so that the videos obtained when UAVs execute planned routes satisfy end-user requirements. These requirements have been provided by *e-distribución*[2], the largest electric power distribution company in Spain, and range from the relative position that the UAV camera should keep with respect to the power grid to coverage requirements.
2. Accurate model of battery consumption used to plan feasible routes that can be completed by their assigned UAVs. This model captures the effect on the energy consumption of the UAV mass, the inspection speed and the weather conditions (temperature, atmospheric pressure, and wind magnitude and direction), among other relevant parameters that are frequently neglected. The presented model has been validated using statistical results extracted from flight experiments.
3. Unified software framework for effective field operation. The proposed approach introduces and integrates several software modules to address specific aspects that arise when intended for usage in real-world conditions. These modules include a GUI (Graphical User Interface) to easily set up and launch mission planning, the integration of third-party APIs (Application Programming Interfaces) to obtain both real-time weather forecasts to feed the consumption model and terrain elevation models to accurately locate transmission towers, along with the software that enables autonomous mission execution and monitoring. All of this software has been released as open source.
4. Flight experiments in real-world conditions. The integrated solution presented in this paper was successfully tested during the final live demonstration of the European project AERIAL-CORE. A heterogeneous multi-UAV team was able to autonomously inspect a real power grid consisting of more than 10 kilometres of overhead power lines with several forks in 13 minutes, while streaming the captured videos to a GCS (Ground Control Station) and identifying a simulated power outage and its exact location.

The subsequent sections of the manuscript are structured as follows. Firstly, Section 2 describes the multi-UAV inspection problem. Secondly, Section 3 models the previous problem, focusing on a graph-based abstraction of it, a clustering method to simplify the resulting graph, and the derivation of a model of battery consumption for UAVs. Next, Section 4 is devoted to the multi-UAV route planning method for fast inspection of overhead power grids. Then, Section 5 addresses the main aspects that should be faced for an effective field operation of the approach proposed in this paper. Section 6 shows a general view of the resulting integrated solution and the connections between its main modules introduced before. Once the complete framework is presented, Section 7 validates it through flight experiments in real-world conditions and compares it to the state of the art. Finally, Section 8 summarises the conclusions.

[2] https://www.edistribucion.com/

2 The Multi-UAV Inspection Problem

This article concentrates on the autonomous inspection of overhead power grids using a fleet of UAVs endowed with cameras while minimising the mission time. These power grids are composed of transmission towers and the connecting wires, and their characteristics are usually known, including the tower coordinates (latitude and longitude), their type and size, and the wiring between them. Regarding the UAVs, they may have heterogeneous capabilities in terms of battery consumption and flight speed, and commanded and supervised from a centralised GCS, each of them operates from a station where it takes off and lands safely, existing also the possibility of recharging batteries autonomously by contact for extended operations (see Fig. 2).

An inspection mission starts with the UAVs waiting for a mission in their respective stations and consists of several steps. Firstly, a route planning method computes the best inspection sequence for each UAV. Then, the UAVs should track the plan autonomously while they stream the captured videos to a GCS. This information is also recorded on board the aerial robots. Simultaneously, the transmitted information can be analysed in real time by an operator specialised in this task to detect defects or failures. Finally, the mission finishes when all the UAVs return to their stations after completing the grid inspection.

Concerning the effectiveness of the inspection, the videos obtained by the UAVs must satisfy end-user requirements. These requirements are based on those used in current inspections conducted from manned helicopters (see Fig. 3). The main requirements can be enumerated as follows.

Fig. 2 Multi-rotor UAV and its station for safe take-off, landing, and autonomous battery recharging by contact

Fig. 3 Video snapshot from a current inspection conducted using a manned helicopter

Requirement 1 (Video perspective). *The relative position that the UAV camera must keep with respect to the power grid (both distance and orientation) has to be adjusted to ensure that a good perspective of the power-grid elements can be captured during the inspection. This adjustment involves moving the flight path laterally with respect to the power-line axis, so that the angle between the shortest segment connecting the UAV camera to the power line and the line perpendicular to the ground is approximately 45 degrees. Although it is easier to capture a zenithal perspective (0 degrees) since it involves flying directly over the tower coordinates at a certain altitude, this perspective does not offer, for example, a clear view of the distance between vegetation on the ground and the power-line cables.*

Requirement 2 (Power-grid coverage). *The UAV videos must capture all the elements of the power grid and its surroundings, including transmission towers and their foundations, cables, vegetation, buildings, and potential defects, while ensuring continuous videos that cover the entire length of the power lines.*

Requirement 3 (Defect location). *The video frames must be georeferenced at all times in order to identify the exact location of any defect that might be found in the power grid, either during the mission execution or in subsequent post-processing of the recorded videos.*

3 Problem Modelling

This section is devoted to modelling the problem described above, as the route planner presented later in Section 4 is built upon the derived models. As described hereinafter, the modelling focuses on three aspects: a graph-based abstraction of the inspection problem, a clustering method that can be used to simplify the resulting graph, and the formulation of a battery consumption model for UAVs.

3.1 Inspection Graph

This paper utilises graph theory to model the multi-UAV inspection problem. Given the power grid to be covered, where the locations of its transmission towers and their interconnections are known, along with the available UAVs and the coordinates of their stations as inputs, a graph-based abstraction of the inspection problem can be derived. Specifically, the problem can be modelled using a directed weighted multigraph $\mathcal{G} = (\mathcal{V}, \mathcal{E}, \mathcal{W}, \mathcal{D})$, which is depicted with a simple example in Fig. 4 and explained in detail below.

The set $\mathcal{V} = \mathcal{P} \cup \mathcal{O}$ represents the graph nodes and consists of two components: the set of n transmission towers $\mathcal{P} = \{1, 2, ..., n\}$, and the set of δ UAV stations $\mathcal{O} = \{0_1, 0_2, ..., 0_\delta\}$, where δ denotes the number of agents available in the multi-UAV team. This team is represented by the set $\mathcal{D}$, with $|\mathcal{D}| = \delta$.

The nodes in $\mathcal{V}$ are connected by the set of edges $\mathcal{E}$, representing possible UAV flight paths between these nodes. Associated with the edges in $\mathcal{E}$, there is the set of costs $\mathcal{W} = \mathcal{T} \cup \mathcal{B}$, where the sets $\mathcal{T}$ and $\mathcal{B}$ correspond to the costs in terms of flight time and battery consumption between nodes, respectively. The flight times are calculated based on the UAV flight speeds during the inspection and the locations of the electric towers and the UAV stations. Additionally, when the UAVs return to their stations for battery recharging, the charging duration is factored into the total flight time. Battery consumption calculations are addressed later in Section 3.3.

Regarding the number of edges between two nodes and their characteristics, two key aspects must be taken into account. First, since the UAVs may be heterogeneous, the flight cost between two nodes varies depending on the specific UAV used. Second, the flight cost may also be influenced by the flight direction, for instance, due to wind conditions. As a result, the number of edges connecting two nodes is

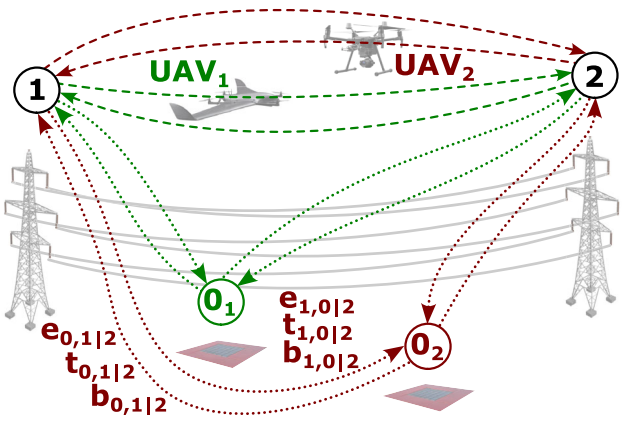

Fig. 4 Graph-based abstraction of the multi-UAV inspection problem. Simple example with two connected towers and two heterogeneous UAVs

$2 \times \delta$, except in cases where one node belongs to the set $\mathcal{O}$, since each UAV must operate from its designated station. In these cases, the number of edges is 2. Nodes within the set $\mathcal{O}$ are not connected between them. Thus, the edge $e_{i,j|k} \in \mathcal{E}$ represents the possible flight of UAV k from node i to node j ($i \neq j$), which takes time $t_{i,j|k} \in \mathcal{T}$ and uses battery energy $b_{i,j|k} \in \mathcal{B}$, normalised relative to full battery capacity. Generally, $t_{i,j|k} \neq t_{j,i|k}$ and $b_{i,j|k} \neq b_{j,i|k}$, as well as $t_{i,j|k} \neq t_{i,j|q}$ and $b_{i,j|k} \neq b_{i,j|q}$, where $q \in \mathcal{D}$ and $q \neq k$.

Despite the previous considerations, the edges in $\mathcal{E}$ can be divided into two distinct sets: $\mathcal{E} = \mathcal{C} \cup \mathcal{U}$. On one hand, the set $\mathcal{C}$ comprises all edges connecting two nodes within the set $\mathcal{P}$, when these nodes represent transmission towers that are physically connected in the actual power grid, as shown in Fig. 4 for nodes 1 and 2 (dashed edges). On the other hand, the set $\mathcal{U}$ consists of the remaining edges not included in $\mathcal{C}$ (dotted edges in Fig. 4).

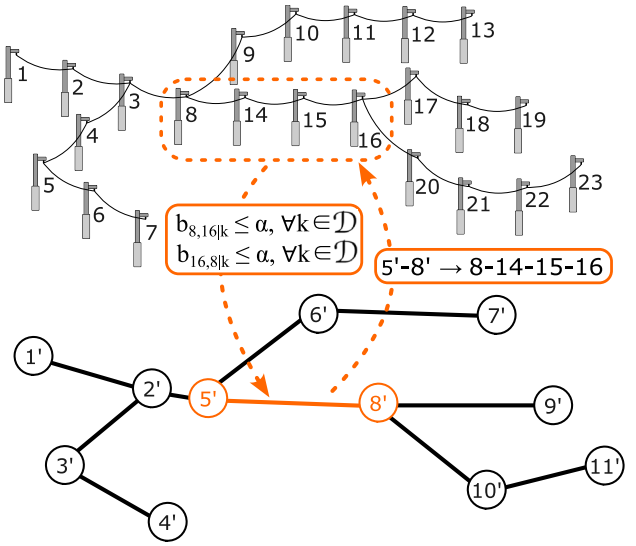

Fig. 5 Graphical representation of the clustering method: original (top) and clustered (bottom) power grids

3.2 Power-Grid Clustering

The search for optimal solutions in graphs like the one presented in the previous subsection is widely recognised as an NP-hard (Non-deterministic Polynomial-time hard) problem, where the computational load escalates drastically as the number of vehicles and nodes increases. As a result, finding exact solutions within a reasonable time becomes challenging as the problem size grows. To tackle this issue, heuristic methods are commonly employed [22]. These methods provide alternative strategies for the optimisation process, yielding suboptimal solutions that are acceptable within bounded computation times. In addition to reducing computational complexity through heuristics, another approach is the adoption of clustering methods [23], which can help to simplify the graph representation of the multi-UAV inspection problem.

A clustering method was first proposed in the previous paper of the authors [21], and its operation basis has been outlined here for the sake of completeness. As depicted in Fig. 5, the clustering method groups segments of the power grid located within the same branches based on a consumption criterion, creating simplified branches that represent the original ones. Thus, every cluster ensures that the battery threshold $\alpha \in (0, 1)$ is never exceeded for any UAV in the set $\mathcal{D}$. It is important to note that this process maintains traceability between the edges of original and clustered power grids as illustrated in Fig. 5. Therefore, route planning can be formulated on the simplified graph and, once a solution is found, this can be represented in relation to the original power grid. For more details about this clustering method, please refer to Section IV in paper [21].

3.3 Battery Consumption

The graph-based abstraction presented in Section 3.1 associates estimates of battery consumption with the edges in the graph. These costs will be used for route planning, and consequently, the feasibility of the computed solutions will depend on the accuracy of the cost estimates. For this reason, this section introduces a model of energy consumption designed to accurately estimate the electric power required by multi-rotor UAVs when flying between transmission towers and stations, and by extension, the level of battery that is drained. This model captures the impact on the energy consumption of UAV mass, inspection speed, and weather conditions (temperature, atmospheric pressure, and wind magnitude and direction), among other relevant parameters that are often overlooked.

Since most of the flight time in missions like inspections of power grids is spent flying horizontally at constant speed over inspection targets, the presented consumption model focuses on forward flights. Moreover, short transitions involving axial flights, such as ascent and descent during take-off and landing, do not significantly contribute to the total consumption in such missions as they usually represent less than 5% of the total flight time (e.g., 1-2 minutes in missions around 40 minutes), and practical applications have shown that these axial transitions are typically performed at low speeds. Consequently, the associated energy consumption is similar to the consumption in hovering flight conditions [24, 25], which is a particular case of forward flight with a forward speed equal to zero.

The model of energy consumption described here is based on energy principles and makes use of the aerodynamic power in its derivation. Thus, starting from the set of parameters listed in Table 1, the different components of the aerodynamic power required for any given mission can be estimated. Then, the Principle of Conservation of Energy can be leveraged to obtain the associated electric power demanded from the UAV batteries. Finally, the battery charge required to satisfy the electricity demand can be deduced from such electric power. More details are provided below.

Inspired by the Principles of Helicopter Aerodynamics [24], the aerodynamic power P_a of a multi-rotor UAV can be modelled as

$$P_a = n_r(P_i + P_0) + P_f \tag{1}$$

where P_i is the induced power to speed up the rotor airflow and produce thrust, P_0 is the profile power associated with the drag of the rotor blades, and P_f is the parasitic power required to counteract the drag of the airframe. In contrast to other simplified consumption models used for planning purposes, where the aerodynamic power is frequently estimated only for hover conditions and the contributions of the blade profile power and the parasitic power are neglected, the model presented here is more complex but leads to more accurate estimates.

Concerning the induced power P_i for each rotor, there is the following relation with the thrust T exerted by the rotor and its induced velocity v_i

$$P_i = \kappa T v_i \tag{2}$$

Table 1 Parameters used as inputs in the model of battery consumption

Parameter	Description
m	UAV mass (including payload)
g	Gravity acceleration
n_r	Number of rotors
n_b	Number of rotor blades
R	Radius of the rotors
c	Blade chord
Q	Battery energy
C_l	Lift coefficient (rotor blade)
C_d	Drag coefficient (rotor blade)
ρ	Air density
f	Equivalent flat-plate area (fuselage)
κ	Induced power factor
K_μ	Numerical constant
η	Aerodynamic efficiency

Additionally, according to the Momentum Theory [24], the induced velocity v_i fulfils

$$v_i = \Gamma - v_\infty sin(\alpha_r), \tag{3}$$

where v_∞ is the UAV airspeed, α_r the angle of attack of the rotors and Γ a variable whose value can be computed using again the Momentum Theory from

$$\Gamma - v_\infty sin(\alpha_r) - \frac{T}{2\rho\pi R^2\sqrt{v_\infty^2 cos^2(\alpha_r) + \Gamma^2}} = 0\ . \tag{4}$$

Going back to Equations (2)-(4), the thrust T and the angle of attack α_r can be computed by establishing equilibrium of forces for the vehicle in forward flight

$$T = \frac{mg}{n_r cos(\alpha_r)} \tag{5}$$

$$tan\,(\alpha_r) = \frac{D}{mg}\ , \tag{6}$$

being D the drag of the airframe, which can be modelled as

$$D = \frac{1}{2}\rho v_\infty^2 f\ . \tag{7}$$

The parameter f is known as the equivalent flat-plate area and accounts for the drag of the airframe [24]. It may be defined as $f = C_{D_f} S_{ref}$, where S_{ref} is a reference area whose definition may not be unique, and C_{D_f} is the airframe drag coefficient based on that reference area. However, the direct use of the parameter f helps to avoid potential ambiguities associated with the choice of S_{ref}.

Regarding the blade profile power P_0, the application of the Blade Element Theory [24] gives rise to

$$P_0 = \frac{\rho R^4 \Omega^3 n_b c C_d}{8}\left(1 + K_\mu\left(\frac{v_\infty cos(\alpha_r)}{\Omega R}\right)^2\right) \tag{8}$$

$$\Omega = \sqrt{\frac{6T}{\rho n_b c R^3 C_l} - \frac{3}{2}\left(\frac{v_\infty cos(\alpha_r)}{R}\right)^2}\ , \tag{9}$$

where Ω is the rotational speed of the rotors.

Switching to the parasitic power P_f, this is by definition

$$P_f = D v_\infty\ . \tag{10}$$

Once the aerodynamic power P_a used to lift the vehicle is computed, the electric power P_e generated by the UAV batteries can be estimated through the Law of Conservation of Energy. According to this law, the electric power P_e is transformed into the aerodynamic power P_a, with certain

power losses quantified through the efficiency parameter η. Consequently,

$$Pe = \frac{P_a}{\eta} \ . \tag{11}$$

where the aerodynamic efficiency η can be considered a constant parameter, as it has been demonstrated for motor-propeller combinations recommended by manufacturers and working at typical operating conditions [26].

Finally, the battery charge E_e, referenced with respect to the maximum battery capacity Q ($E_e \in [0, 1]$), required to provide the electric power P_e during a flight time Δt can be deduced from

$$E_e = \frac{1}{Q} \int_0^{\Delta t} P_e dt \ . \tag{12}$$

This battery charge E_e is used for the graph-based representation of the inspection problem, giving the values of $b_{i,j|k}$ in Section 3.1.

Figure 6 shows the evolution of the electric power P_e, computed according to previous equations, with respect to the airspeed v_∞ and the mass m for a standard UAV. As can be observed, the electric power decreases with increasing low forward speeds [27]. In contrast, this power increases dramatically at high speeds due to parasitic losses. The combination of both effects leads to the existence of an optimal value for the forward speed that maximises the time that the vehicle can fly without recharging batteries. Based on [24], an estimate of this optimal forward speed v_∞^* adapted to multi-rotor UAVs is given by

$$v_\infty^* = \sqrt{\frac{mg}{\rho \pi R^2}} \left(\frac{\kappa \pi R^2}{3 n_r f} \right)^{1/4} \ . \tag{13}$$

Aligned with the latter, the results demonstrate that other simplified models, such as the one adopted in [25], where the aerodynamic power is always approximated by the one required in hover conditions ($v_\infty = 0$), give an overestimate of the electric power. Although those models could be assumed valid for low speeds and imply estimates on the side of safety, they may result in significant errors. Figure 6 also shows how the electric power always increases with the UAV mass, which is an expected phenomenon.

The airspeed v_∞ used in the previous derivations is the relative horizontal speed that the UAV experiences with respect to the air. However, the ground speed v_g is used in this paper as a reference since it is directly related to the speed that ensures a proper information capture due to camera sensor limitations. The relation between both air and ground speeds is given by

$$v_\infty = \sqrt{v_g^2 + v_w^2 - 2 v_g v_w cos(\theta_w)} \ , \tag{14}$$

where v_w is the wind speed, and θ_w is the angle between the ground speed and the wind speed vectors. This equation means that both speeds coincide only when there is no wind. In the rest of the cases, flying at certain ground speed implies that the wind has an effect on the energy consumption. This effect can be beneficial or not depending on the magnitude

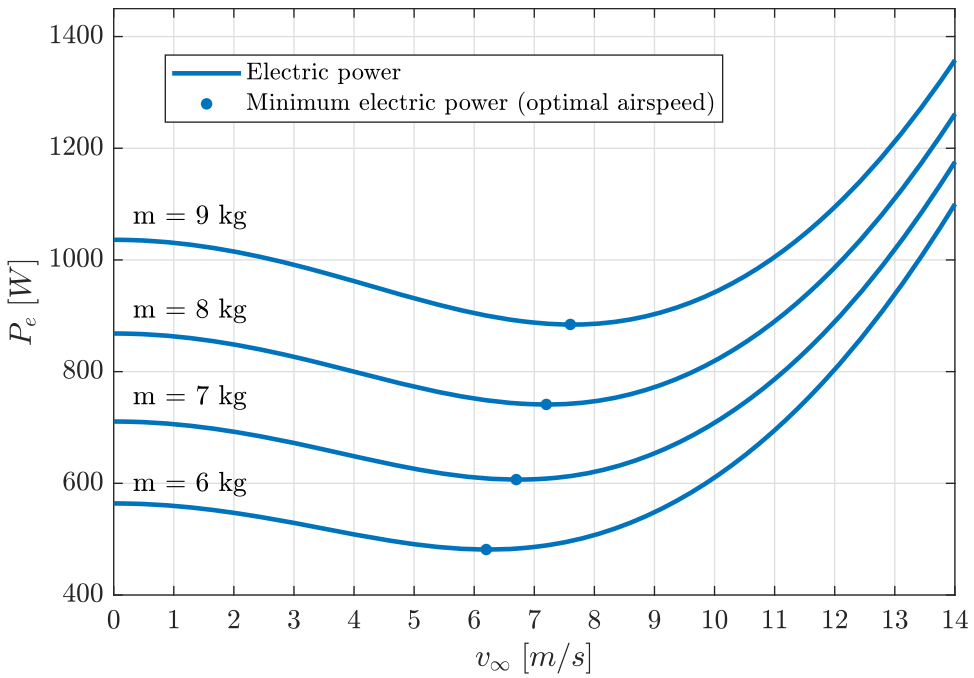

Fig. 6 Evolution of the electric power P_e demanded by a standard UAV with respect to its forward airspeed v_∞ and its mass m

and orientation of the wind with respect to the UAV movement and can be estimated by integrating Equation (14) into Equations (1)-(12).

It should be highlighted that the effect on the battery consumption of other weather variables like temperature T and atmospheric pressure p is also captured in the derived model through the air density ρ. In this sense, the Ideal Gas Law offers the following relation that can be adopted here

$$\rho = \frac{M_m p}{R_g T}\ , \tag{15}$$

where M_m is the molar mass of the air, and R_g is the universal gas constant. Other simplified models like the ISA (International Standard Atmosphere) model assume fixed standard-day temperature and pressure and therefore cannot capture meteorological variations (e.g., barometric fluctuations due to wind conditions, or daily temperature swings) that significantly affect the power consumption through the air density. To provide more accurate energy estimates, Equation (15) needs to be retained, computing density from the actual ambient pressure and temperature measurements rather than from nominal values.

4 Route Planning

The calculation of efficient routes for the inspection of overhead power lines by only one UAV tends to be relatively simple, but such inspections may require significant time to be completed. To overcome this limitation, multi-UAV strategies are commonly implemented to accelerate the inspection. However, determining optimal routes that minimise the overall mission duration becomes more challenging when power grids have complex topologies and multiple UAVs, potentially with heterogeneous capabilities in battery consumption and flight speed, are involved. In this context, this section presents a route planning approach designed to compute the optimal assignment and inspection sequence for each aerial robot.

4.1 Capacitated Min-Max Multi-Depot Vehicle Routing Problem

Starting from the graph-based abstraction presented in Section 3.1, or its clustered version according to Section 3.2, the inspection mission can be reformulated as an optimisation problem on the graph $\mathcal{G}$, where the optimal assignment and inspection sequence must be determined for each UAV. Specifically, each UAV in set $\mathcal{D}$ starts and finishes at its station in set $\mathcal{O}$, flying between the nodes in set $\mathcal{P}$ to fully cover all edges in the set $\mathcal{C}$, either in one direction or in the opposite, within the shortest mission time as determined by the costs in set $\mathcal{T}$. This must be achieved while respecting the UAV battery capacity constraints, verified using the costs in set $\mathcal{B}$ and computed according to Section 3.3. This implies that if the inspection task exceeds the UAV ranges on a single battery charge, they must return to their stations to recharge the batteries before resuming the mission.

The problem outlined above can be approached as a variant of the VRP, named here capacitated (UAVs with limited battery) min-max (minimisation of the inspection time for the UAV that takes the longest time) multi-depot (UAVs operating from different stations) VRP, and its exact solution can be obtained using MILP (Mixed Integer Linear Programming). To achieve this, a set of decision variables $\mathcal{X}$ needs to be defined, where the binary variables $x_{i,j|k} \in \mathcal{X}$ indicate whether the edges $e_{i,j|k} \in \mathcal{E}$ are covered ($x_{i,j|k} = 1$) or not ($x_{i,j|k} = 0$). Additionally, it should be noted that optimising the mission duration for the multi-UAV team requires minimising the inspection time of the UAV that takes the longest time to complete its route, as the mission concludes only once the last UAV has returned to its station. To accommodate this min-max objective, which is inherently nonlinear, the objective can be reformulated for MILP by minimising the sum of inspection times for all UAVs, while aiming to keep these times balanced. To incorporate this balance within the optimisation problem, real variables $y_{r,q} \geq 0$ are introduced for each pair of UAVs r and q in set $\mathcal{D}$, where $r < q$. These variables capture the differences in inspection times between the pairs of UAVs indicated by their subscripts (e.g., between the pairs of agents {1, 2}, {1, 3} and {2, 3} if there are 3 available UAVs).

Taking into account all the preceding aspects, the MILP problem can be presented in the following manner

$$\underset{x_{i,j|k}, y_{r,q}}{min} \sum_{\substack{\{i,j\}\in\mathcal{V} \\ i\neq j \\ k\in\mathcal{D}}} t_{i,j|k} x_{i,j|k} + \sum_{\substack{\{r,q\}\in\mathcal{D} \\ r<q}} y_{r,q} \tag{16}$$

$s.t.$

$$\sum_{j\in\mathcal{P}} x_{0_k,j|k} \geq 1 \quad \forall k \in \mathcal{D} \tag{17}$$

$$\sum_{i\in\mathcal{P}} x_{i,0_k|k} \geq 1 \quad \forall k \in \mathcal{D} \tag{18}$$

$$\sum_{\substack{j\in\mathcal{V} \\ j\neq i}} \left(x_{i,j|k} - x_{j,i|k}\right) = 0 \quad \forall i \in \mathcal{V}, \forall k \in \mathcal{D} \tag{19}$$

$$\sum_{k\in\mathcal{D}} \left(x_{i,j|k} + x_{j,i|k}\right) \geq 1 \quad \forall \{i,j\} | e_{i,j|k} \in \mathcal{C}, i < j \tag{20}$$

$$\sum_{\substack{\{i,j\}\in\mathcal{V} \\ i\neq j}} \left(t_{i,j|r} x_{i,j|r} - t_{i,j|q} x_{i,j|q}\right) - y_{r,q} \leq 0$$
$$\forall \{r,q\} \in \mathcal{D}, r < q \tag{21}$$

$$\sum_{\substack{\{i,j\}\in\mathcal{V}\\ i\neq j}} \left(t_{i,j|q}x_{i,j|q} - t_{i,j|r}x_{i,j|r}\right) - y_{r,q} \leq 0$$

$$\forall\{r,q\} \in \mathcal{D}, r < q \tag{22}$$

$$\sum_{\substack{i\in\mathcal{S}\\ j\notin\mathcal{S}\\ k\in\mathcal{D}}} \left(x_{i,j|k} + x_{j,i|k}\right) \geq 2h(\mathcal{S}) \quad \forall\mathcal{S} \subset \mathcal{P} \tag{23}$$

In this formulation, the objective function in Equation (16) aligns with the optimisation approach outlined before. Constraints (17) and (18) ensure that all UAVs start and finish the mission at their designated stations. These constraints also permit UAVs to revisit the stations if battery recharging is needed. Constraints (19) maintain continuity at each node for each UAV, meaning that if a UAV reaches a node, it must also depart from that node. Constraints (20) ensure full coverage of the power grid, as they require at least one edge between every pair of connected towers in set $\mathcal{C}$ to be chosen, in either direction. Constraints (21) and (22) are set to balance inspection times between UAVs. By including the sum of decision variables $y_{r,q}$ in the objective function, minimising this sum enforces minimisation of individual $y_{r,q}$ values, thereby balancing inspection times for each UAV pair r and q according to these constraints. Finally, Constraints (23) are commonly known as the subtour elimination constraints and their implementation has been widely studied in the literature [28, 29]. They prevent the creation of subtours unconnected to any station or tours that surpass the UAV battery capacities. Here, the function $h(\mathcal{S})$ provides a lower bound on the UAV entries and exits that every subset $\mathcal{S}$ in $\mathcal{P}$ requires. However, as the number of subsets $\mathcal{S}$ can be substantial, these constraints are generally omitted initially and added incrementally when unmet [30]. To further expedite the optimisation process, these additional battery constraints can also be incorporated

$$\sum_{\substack{\{i,j\}\in\mathcal{V}\\ i\neq j}} b_{i,j|k}x_{i,j|k} \leq \sum_{j\in\mathcal{P}} x_{0_k,j|k} \quad \forall k \in \mathcal{D} \tag{24}$$

These constraints require that the total battery consumed by each UAV along its operation (left-hand side of the inequality) does not exceed the number of times it departs from its station (right-hand side of the inequality), under the assumption that the UAVs always leave their stations with fully charged batteries.

4.2 Route Reconstruction

The solution of the MILP problem in the previous subsection provides the set of decision variables $x_{i,j|k}$ with a binary value of 1, thus yielding the set $\mathcal{E}^*$ of selected graph edges $e^*_{i,j|k}$ to be covered by the multi-UAV team. Next, the edges $e^*_{i,j|k}$ assigned to a particular UAV k can be easily identified, as these are already indexed by k. Subsequently, the inspection sequence for each UAV k can be determined in order by starting from its edge $e^*_{i,j|k}$ where index i is equal to 0_k and sequentially linking edges until reaching its edge $e^*_{i,j|k}$ where j equals 0_k. In cases where multiple edges $e^*_{i,j|k}$ have indices i equal to 0_k for the same UAV k, this indicates the presence of multiple tours for that UAV. Nevertheless, all these tours can be handled as a single multi-tour sequence, assembled by linking each tour through the node 0_k. This approach ultimately provides each UAV k with an optimised route $\mathcal{R}_k$, represented as a sorted set of nodes directly derived from the preceding edge sequence, as follows

$$\mathcal{R}_k = \{0_k, A, B..., C, ..., D, E, 0_k\} \quad \forall k \in \mathcal{D}, \tag{25}$$

where A, B, C, D, and E represent the nodes (transmission towers) that UAV k must visit during the inspection mission. Nodes such as B, C, or D may also represent the station 0_k.

5 Considerations for Effective Field Operation

The approach introduced so far establishes a solid strategy to compute feasible routes that can lead the multi-UAV team to the efficient inspection of overhead power grids. Next, the main aspects that must be faced for an effective field operation have been addressed along this section.

5.1 Accurate UAV Positioning

The route planner presented in Section 4 gives the sequences of transmission towers and stations that the UAVs must follow to perform their mission. Then, these sequences must be transformed to the WPs (Waypoints) that every UAV must track. Since the elements in the power grid are the inspection targets, the UAV positioning will be calculated relative to the power-grid location. Therefore, the 3D location of the transmission towers in the grid must be known.

According to information provided by the power distribution company *e-distribución*, the coordinates of the transmission towers (latitude and longitude), their types and sizes, and the wiring between them are commonly stored in accessible databases, but their altitudes are not included. This lack of altitude information may have a limited impact on inspections with a zenithal perspective, as represented in Fig. 7 (left), where inaccuracies in the UAV vertical positioning relative to the power line still allow satisfying coverage requirements. However, these same inaccuracies can lead to ineffective results for inspections according to Requirement 1 in Section 2, as depicted in Fig. 7 (right).

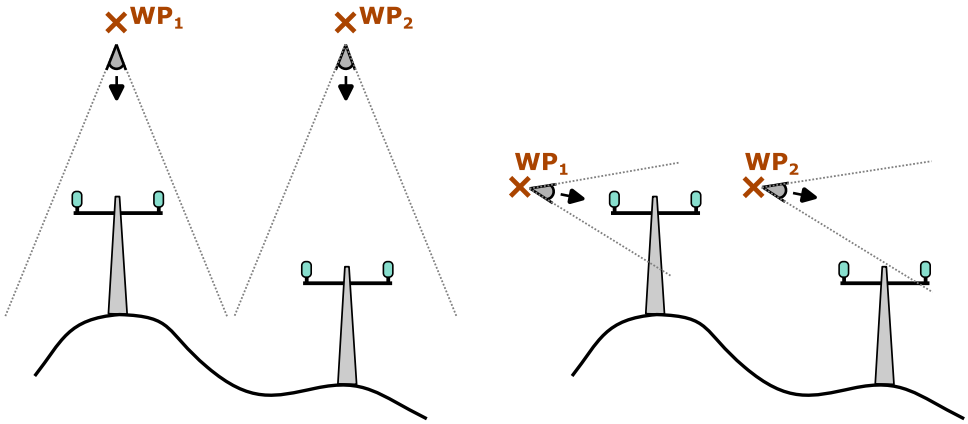

Fig. 7 Effect of tower altitude inaccuracies on UAV inspection: inspection from a zenithal perspective (left), and inspection from a perspective in accordance to end-user requirements (right)

To cope with the issue described above, the third-party API *Open Topo Data*[3] has been integrated to have access to terrain elevation models that help to accurately locate transmission towers. In particular, the *eudem25m* dataset, which covers Europe at a 25-metre resolution and provides a vertical accuracy of 7 metres, has been adopted. This level of accuracy has proven sufficient for practical applications, as will be demonstrated later in Section 7. Other datasets covering various regions around the world are also available. Thus upon request, given the latitude and longitude of the transmission towers and the UAV stations, the API returns their terrain altitudes in a consistent reference frame. Combined with end-user database information, this enables accurate 3D referencing of power grids.

Once the UAV routes are computed and the power grid is properly georeferenced, the final stage consists of calculating the WPs of the UAV paths. Instead of flying directly between WPs over the tower coordinates at a certain height while recording a zenithal perspective, as represented in Fig. 8 (left), the flight path must be offset laterally from the power-line axis to fulfil Requirement 1 in Section 2. At the same time, Requirement 2 in Section 2 cannot be disregarded, and full coverage of the power grid must be guaranteed. To meet both requirements, this paper adopts the approach illustrated in Fig. 8 (right). WPs are computed so that the flight path is always parallel to the power-line axis, with the UAV camera oriented perpendicular to it, and every power-line segment between two transmission towers is fully covered, including the towers themselves. The flight height is adjusted relative to the power-line elevation to keep the camera perspective provided by the end user.

Finally, it should be mentioned that Requirement 3 in Section 2 is also satisfied by recording the inspection videos simultaneously with logging the UAV coordinates throughout the path execution, using a common time reference for time stamping.

5.2 Weather Estimates

The model of battery consumption derived in Section 3.3 and used to compute costs for route planning requires values of air density ρ in the operation area, or alternatively, temperature T and atmospheric pressure p, according to Equation (15). Wind magnitude v_w and direction θ_w are also needed. In order to obtain these values, the third-party API *Weather API*[4] has been integrated. Given the coordinates of any location, this API automatically provides real-time weather data through a network of global weather station collaborations and high-resolution local weather models. Future forecasts can also be requested to assist in planning forthcoming operations.

Alternatively to the use of the previous API, weather information can also be entered manually. This option allows, for example, the use of weather measurements gathered from a meteorological station deployed on site or any other source.

5.3 Graphical User Interface for Mission Planning

The planning strategy presented in this paper can be complemented with a GUI that helps operators to simplify the planning process by intuitively setting up the inspection problem and visually verifying the planning results. This will reduce the probability of human errors while enhancing safety before the mission execution. In this regard, a GUI for mission planning has been developed and introduced in this subsection.

Figure 9 shows a general view of the GUI for mission planning, which has been developed using *Matlab R2023a* and runs on any operating system compatible with this software. The window of this GUI consists of a central display

[3] https://www.opentopodata.org/

[4] https://www.weatherapi.com/

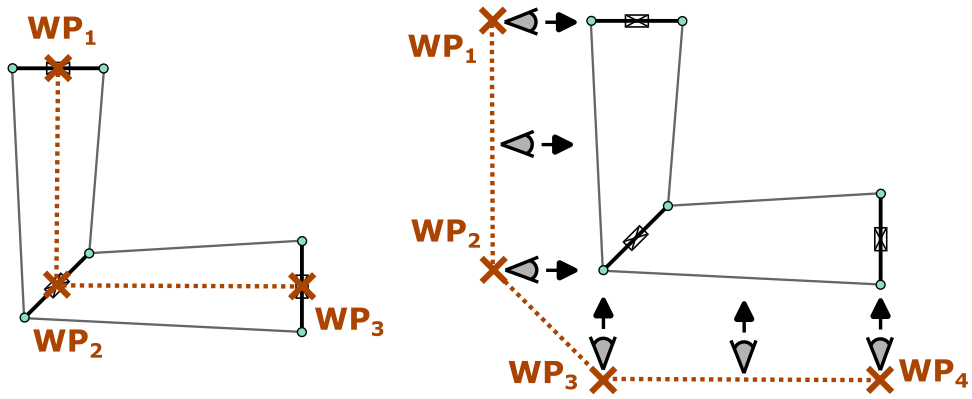

Fig. 8 Waypoint locations to fully cover the power grid: zenithal perspective (left), and lateral perspective (right)

where the scenario (transmission towers, connections, and UAV stations) and the UAV plans are plotted. Surrounding this representation, a set of buttons and text boxes allows the user to interactively set up the inspection problem. Thus, the planning process can be completed following several steps. Firstly, the power-grid map, the available UAVs, and their station locations can be loaded from an inspection database (first panel on the right side) and all related information is shown either graphically in the central display or as text on its left side. Secondly, mission parameters such as the

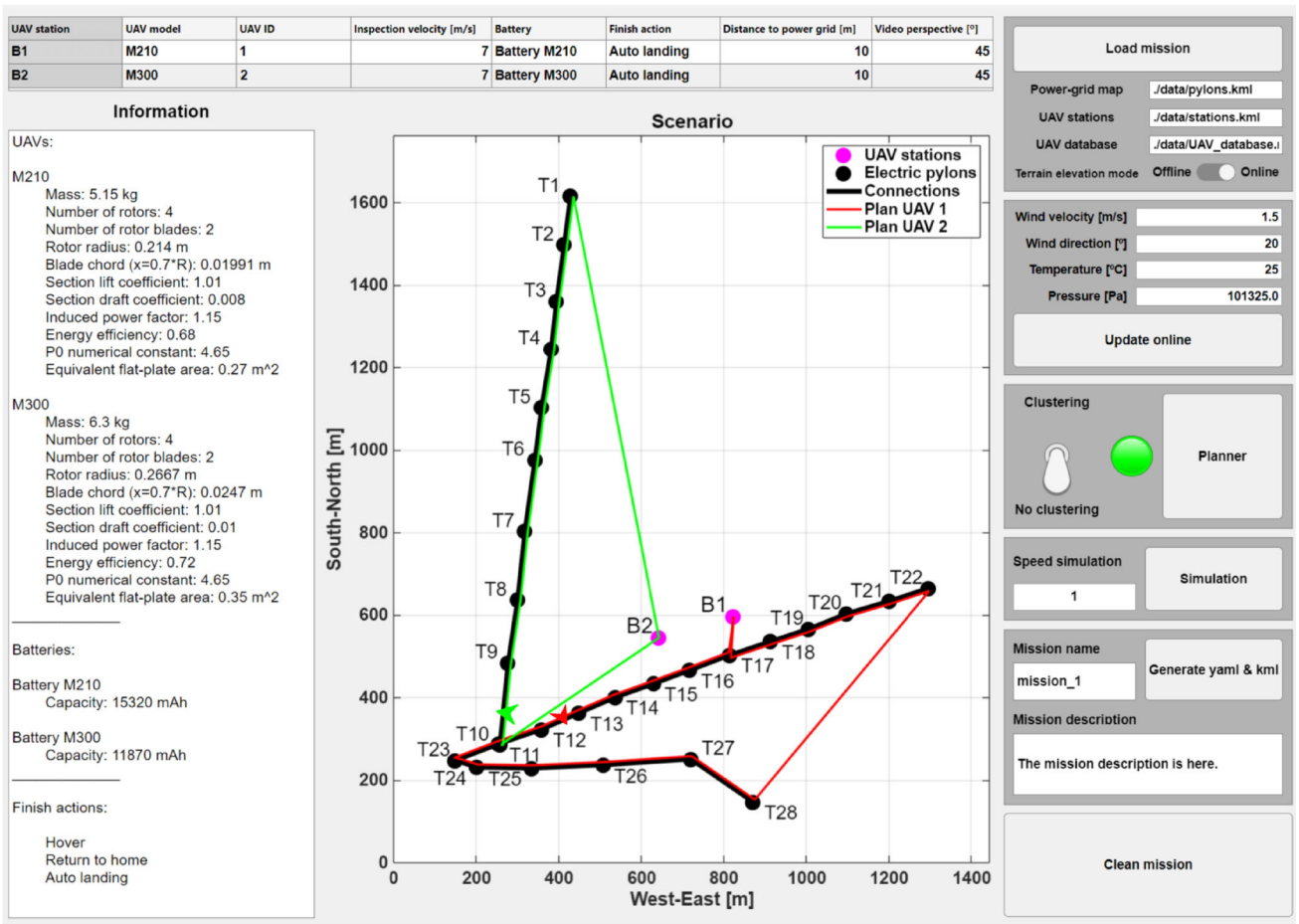

Fig. 9 Graphical User Interface for mission planning

inspection speed or the distance and video perspective of the UAVs relative to the power grid can be configured (top left panel). Thirdly, weather information can either be updated using the API described in Section 5.2, or entered manually, for example, using weather measurements gathered from a meteorological station deployed on site (second panel on the right side). Next, the planner can be launched, enabling automatic power-grid clustering or not (third panel on the right side), and the generated UAV paths are represented in the central display. A simulation that shows a simplified evolution of the UAV flights can also be run to detect potential issues during the mission execution at an earlier stage (fourth panel on the right side). Finally, the plans can be saved for storage in the inspection database and sent for mission execution (fifth panel on the right side).

The GUI presented here, along with the rest of the software developed in this paper for mission planning, has been released as open source[5]. For detailed instructions on its usage, please refer to the documentation included in the repository.

5.4 Mission Execution and Monitoring

The success of the power-grid inspection will strongly depend on the mission execution by the UAVs once their plans are computed. Commercial UAVs generally offer better performance and higher levels of reliability, robustness and safety than research-grade aerial robots. In contrast, their autonomous capabilities are often more limited and typically focus on general-purpose missions, such as tracking of moving targets or simple navigation between WPs that must be manually set by an operator, which reduces their flexibility. Seeking to leverage the advantages of both kinds of UAVs, this paper implements the approach presented in [31], where commercial UAVs are equipped with onboard computers that control their autopilots at a high level and run custom software. This software, based on open-source tools, has been specifically designed to meet the particularities of the autonomous inspection of overhead power grids discussed throughout this paper. Both *DJI*[6] autopilots and autopilots compatible with the *MAVLink*[7] protocol, such as *PX4*[8], are supported, which covers a wide range of UAVs on the market. Moreover, the adopted UAV platforms are intrinsically robust and safe, incorporating built-in sense-and-avoid systems that detect potential obstacles and execute collision-avoidance manoeuvres automatically without the need of human intervention.

At the same time, the onboard computers of all aerial robots in the multi-UAV team communicate with a centralised GCS that commands the inspection mission for fully autonomous execution, monitors the team state (UAV positions, battery levels, quality of the communication signals, among others), and receives and displays the georeferenced video streams. Also, this GCS enables the operator to pause or abort the mission execution at any moment and, when necessary, command a safe return-to-home procedure for the UAVs, thereby ensuring an immediate response to any unforeseen contingency or system failure. The GCS introduced in [32] has been adopted since it offers unique characteristics in terms of scalability, adaptability to different types of UAV autopilots through the use of the *Robotic Operating System* (*ROS*) framework [33], and applicability to the inspection of power grids. This GCS also supports connection with other applications, which facilitates the integration with external software such as the planner presented in this paper, multi-UAV collision avoidance methods to increase safety in the inspection [34], the database where the information generated during the inspection is stored, or any other tools that may be available for the comprehensive management of I&M activities on power grids.

6 The Integrated Solution

This section provides an overview of the integrated solution for autonomous multi-UAV inspection of overhead power lines, including the main modules presented in this article and their interconnections. This integrated solution addresses all key aspects that are needed for an effective field operation and only requires one operator to perform the multi-UAV inspection, with intuitive interactions and minimal workload.

Figure 10 shows a general scheme of the integrated solution. According to this figure, the operator starts the mission by setting it up in the GUI for mission planning (Section 5.3). Then, this GUI automatically runs the planning process, which involves the graph-based abstraction of the inspection problem (Section 3.1), the route planning (Section 4), and the generation of the paths that will lead the multi-UAV team to complete the inspection (Section 5.1). Concerning the graph-based abstraction, this representation is done automatically at the mission planning stage using information extracted from a power-grid map and a UAV database. Moreover, this module makes use of the power-grid clustering (Section 3.2) to automatically cluster the power grid, if desired by the operator, and the model of battery consumption (Section 3.3), which receives parameters from the UAV database and

[5] https://github.com/grvc-robotics-lab/multiUAV_planner/

[6] https://www.dji.com/

[7] https://mavlink.io/

[8] https://px4.io/

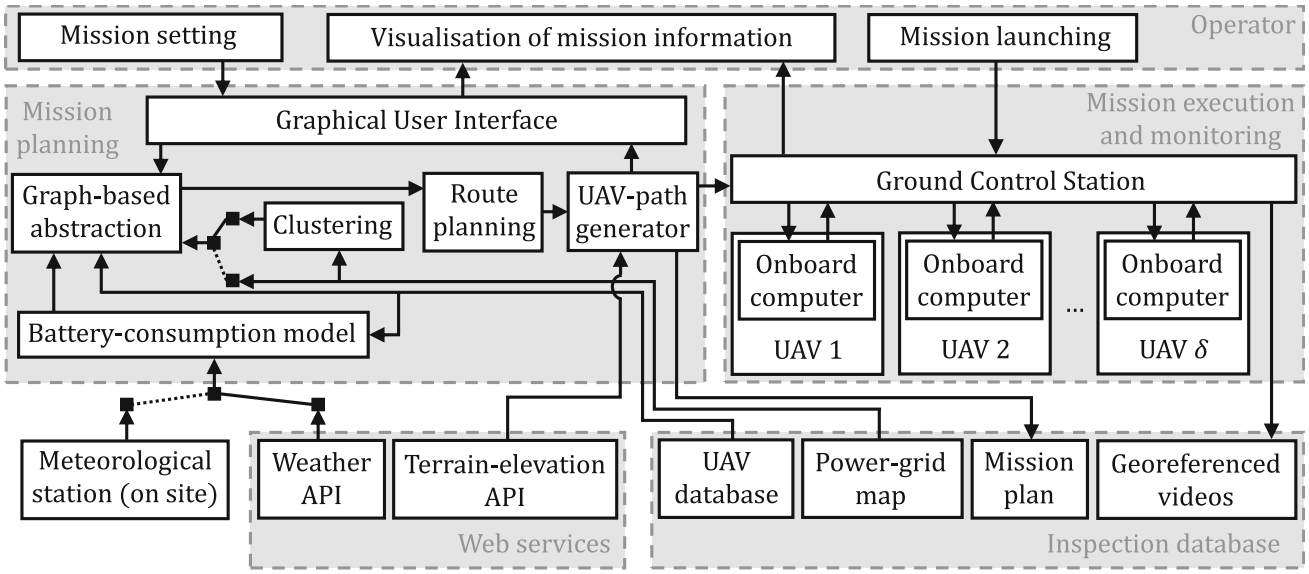

Fig. 10 General scheme of the integrated solution for autonomous multi-UAV inspection of overhead power lines, including the main modules and their interconnections. The arrows indicate how information is exchanged between the different modules, as detailed in Section 6

weather information either from a meteorological station deployed on site, if available, or from the web service accessed through the API for weather estimates (Section 5.2). The API for terrain-elevation models (Section 5.1) is also used for the generation of the UAV paths. Once these paths are computed, they are shared with three modules. Firstly, the paths are displayed on the GUI, enabling the operator to visually verify them. Secondly, the paths are stored in the inspection database and associated with the information generated during the operation in progress. Thirdly, the paths are sent to the Ground Control Station for their subsequent execution.

After completing the mission planning, the operator can start the mission execution and monitoring. To do so, the operator launches the inspection using the GCS (Section 5.4), which distributes the plans among the aerial robots in the multi-UAV team and receives telemetry with the team state through the use of *ROS* topics. Thus, commercial UAVs equipped with onboard computers running custom software are able to perform the inspection autonomously (Section 5.4), while the captured videos are georeferenced and streamed to the GCS. Simultaneously, these videos are displayed for real-time visualisation by the operator and finally stored in the inspection database for post-processing on demand.

7 Experimental Results

This section is dedicated to the experimental validation of the approach presented in this paper. Since the particular capabilities of the algorithm for route planning, including the clustering strategy, were already demonstrated in the previous publication of the authors [21], this section focuses on thoroughly testing the model of battery consumption derived in Section 3.3 and the performance of the integrated solution described in Section 6 when it is applied in real-world conditions.

7.1 Validation of the Battery-Consumption Model

This section validates the model of battery consumption formulated in Section 3.3 by comparing real battery consumptions measured in flight with estimates obtained from the model. For these estimates, the values of the model parameters listed in Table 2 have been used. They correspond to the multi-rotor UAV that has been employed for the

Table 2 Values of the parameters outlined in Table 1 and used for the validation of the consumption model presented in Section 3.3

Parameter	Value	Parameter	Value
m	$7.26kg$	C_l	1.01
g	$9.81m/s^2$	C_d	0.01
n_r	4	ρ	$1.18kg/m^3$
n_b	2	f	$0.35m^2$
R	$0.27m$	κ	1.19
c	$0.025m$	K_μ	4.65
Q	$840000J$	η	0.72

Values obtained from direct measurements, manufacturer data sheets (batteries, propellers), or characteristic tables in [24].

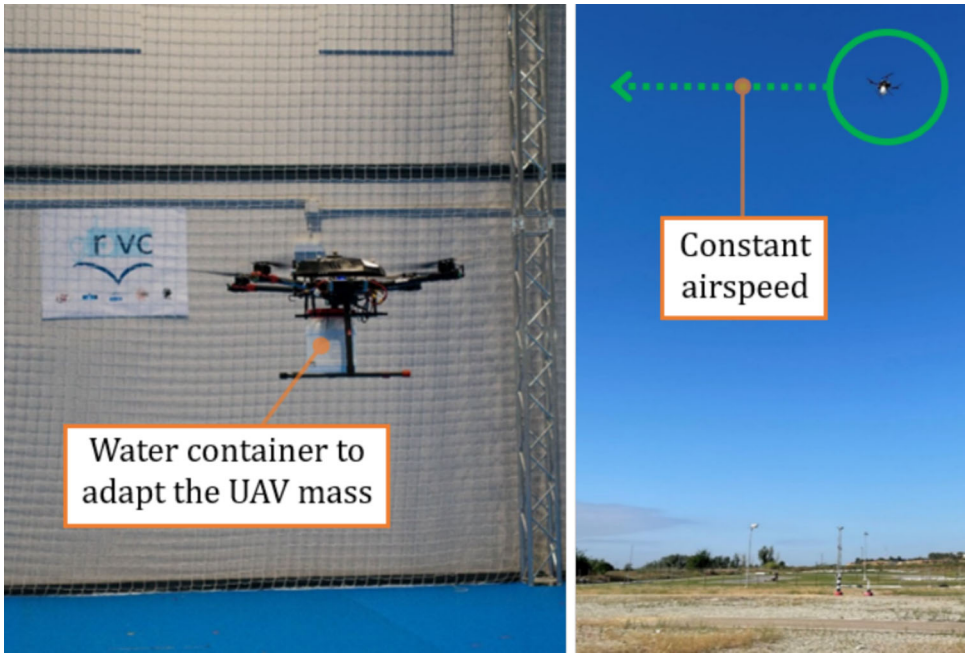

Fig. 11 Setups to measure real battery consumption: flights with different UAV masses (left) and flights with different airspeeds (right)

real flights (see Fig. 11). This aerial robot is a custom-built quad-rotor UAV with autonomous capabilities equipped with a *CAN PMU*[9] power management module that can measure the electric power demanded by the UAV with high accuracy. Additionally, a water container has been attached to the underside of the UAV airframe, allowing its mass to be adjusted on demand for testing purposes by varying the water content.

Regarding the experiments conducted to measure real battery consumptions, two sets of flights have been performed:

1. Flights with different UAV masses. To validate the effect of the mass m on battery consumption, seven flights have been performed with different masses, each repeated three times to obtain statistical results. The masses have been modified by varying the water mass Δm stored in the container attached to the UAV airframe, ranging from $0kg$ to $3kg$. In order to minimise external disturbances while ensuring repeatability and accuracy in the measurements, these experiments have been conducted indoors, in hover conditions (airspeed $v_\infty = 0m/s$), and using an *OptiTrack*[10] motion capture system for accurate UAV positioning. After reaching a steady state, the electric power demanded by the UAV has been logged during a flight time $\Delta t = 20s$ to compute mean values. Figure 11 (left) illustrates the corresponding setup.
2. Flights with different airspeeds. With the focus on validating the effect of the airspeed v_∞ on battery consumption, six flights have been executed at different airspeeds, ranging from $1m/s$ to $6m/s$, with a fixed UAV mass m ($\Delta m = 0kg$), and repeating each of them four

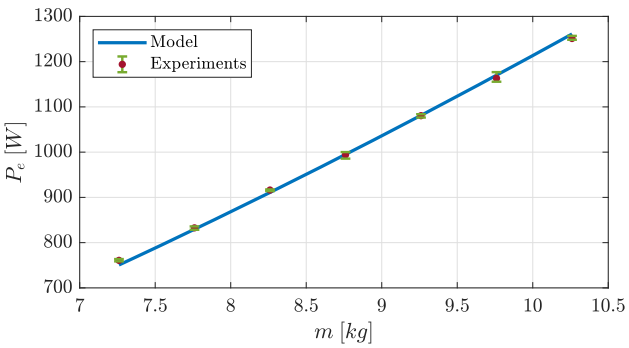

(a) Effect of UAV mass m.

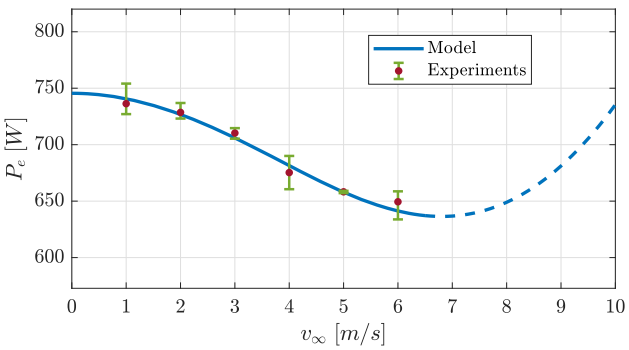

(b) Effect of UAV airspeed v_∞.

Fig. 12 Comparison between the electric power P_e measured in real experiments and estimated using the consumption model presented in Section 3.3

[9] https://doc.cuav.net/power-module/can-pmu/en/

[10] https://www.optitrack.com/

Table 3 Comparison between the battery consumptions E_e^{real}, measured in real experiments, and E_e^{model}, estimated using the consumption model presented in Section 3.3: effect of UAV mass (top) and effect of UAV airspeed (bottom)

Variable mass $m + \Delta m$ (flight time $\Delta t = 20s$, airspeed $v_\infty = 0m/s$)							
Δm	$0.0kg$	$0.5kg$	$1.0kg$	$1.5kg$	$2.0kg$	$2.5kg$	$3.0kg$
E_e^{real}	0.0181	0.0198	0.0218	0.0237	0.0257	0.0277	0.0298
E_e^{model}	0.0179	0.0197	0.0217	0.0237	0.0257	0.0279	0.0300
Relative error	1.34%	0.38%	0.58%	0.09%	0.06%	0.59%	0.79%
Variable airspeed v_∞ (flight time $\Delta t = 20s$, mass m)							
v_∞	$1m/s$	$2m/s$	$3m/s$	$4m/s$	$5m/s$	$6m/s$	
E_e^{real}	0.0175	0.0173	0.0169	0.0161	0.0157	0.0155	
E_e^{model}	0.0176	0.0173	0.0168	0.0162	0.0157	0.0153	
Relative error	0.58%	0.25%	0.62%	0.91%	0.04%	1.26%	

times to obtain statistical results. These flights have been performed outdoors due to space limitations, at times when wind measurements indicated calm conditions to minimise disturbances in the measurements. Straight-line reference trajectories have been autonomously tracked by the UAV during the flights, maintaining constant airspeed and altitude, but varying the flight direction between repetitions to prevent biased measurements caused by residual wind. After reaching a steady state, the electric power demanded by the UAV has been logged during a flight time $\Delta t = 20s$ to compute mean values. Figure 11 (right) shows the associated setup.

The results associated with the previous experiments have been presented in Fig. 12. In these graphs, the blue lines represent the consumption model, while the red dots (mean values) and their corresponding green error bars (minimum and maximum values) depict the statistical results measured during the flights. Based on the graphs, the model fits properly with the flight measurements, showing higher accuracy for flights with variable mass. Nevertheless, this can be attributed to the presence of a higher variability in the measurements from flights with variable airspeed, as outdoor conditions hinder repeatability and introduce small unavoidable disturbances.

Complementing Fig. 12, Table 3 provides a comparison between the battery consumption E_e^{real}, measured during the execution of the experiments, and the estimates E_e^{model}, computed according to Eqs. 1-12. Again, the model predicts the experimental results accurately, showing relative errors that never exceed 1.34%.

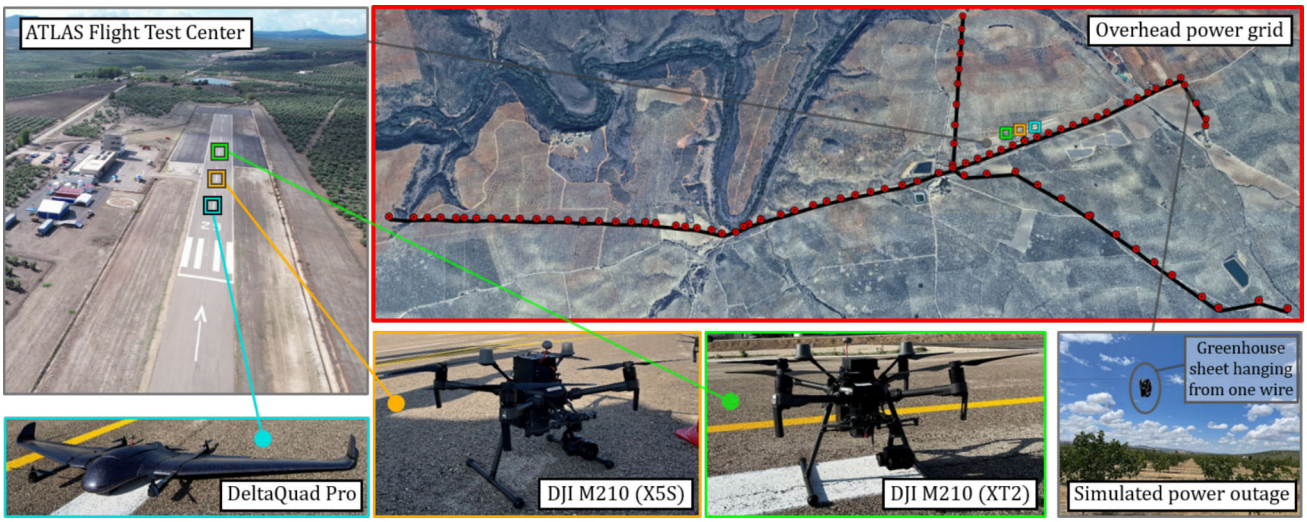

Fig. 13 Experimental setup for the multi-UAV inspection under real-world conditions: overhead power grid to be inspected, with its transmission towers represented as red dots (top right), a piece of greenhouse plastic sheet hanging from one of the wires connecting two towers and simulating a power outage (bottom right), ATLAS Flight Test Center serving as the operation centre (top left) and the heterogeneous team of three UAVs (bottom left)

7.2 Real Power-Grid Inspection

The integrated solution for the inspection of overhead power lines using a multi-UAV team has been experimentally validated under real-world conditions. These experiments were part of the final live demonstration of the European H2020 project AERIAL-CORE, conducted at the ATLAS Flight Test Center[11] (Villacarrillo, Spain). Figure 13 shows the experimental setup. As depicted in the figure, there is an overhead power grid in the surroundings of the centre that stretches for more than 10 kilometres, including multiple forks and 89 transmission towers, marked as red dots in the figure. There, a power outage was simulated at an unknown location of the power grid by hanging a piece of greenhouse plastic sheet from one of the wires connecting two towers. In order to locate the origin of the power outage in minimum time, a team of three heterogeneous UAVs, shown in the figure, was deployed. This team consisted of one fixed-wing UAV with VTOL (Vertical Take-Off and Landing) capabilities, *DeltaQuad Pro*[12], equipped with a *Flir Duo Pro R* camera ($4000 \times 3000 px$ resolution, $56° \times 45°$ field of view), and two multi-rotor UAVs, *DJI M210 RTK*[13], one equipped with the *Zenmuse X5S* camera ($4096 \times 2160 px$ resolution, 72° diagonal field of view) and the other with the *Zenmuse XT2* camera ($3840 \times 2160 px$ resolution, $57.12° \times 42.44°$ field of view). The technical specifications of this multi-UAV team are included in Table 4. Each aerial robot used a *Raspberry Pi 4 Model B*[14] as the onboard computer. The UAVs were deployed along the runway of the ATLAS centre, together with their recharging stations (*Skycharge BOLO S1*[15] docking systems with the setup shown in Fig. 2), while the entire mission was planned, executed, and monitored using a standard laptop (Intel Core i7-1165G7 CPU, 16GB RAM, 512GB SSD, Ubuntu 22.04.3 LTS operating system) operated from the main building of the centre.

The mission began with planning the optimal paths for the multi-UAV team to inspect the entire power grid in minimum time. For this, the GUI for mission planning was used, setting it up with the planning parameters listed in Table 5. For route planning, the MILP problem associated with the capacitated min-max multi-depot VRP was programmed in *Matlab R2023a* and solved using the *intlinprog*[16] solver of the *Optimization Toolbox*. The resulting paths, automatically stored in the inspection database as an exportable *kml* file, are represented in Fig. 14. These paths, computed in 19 seconds, have the characteristics summarised in Table 6 and allow covering the entire power grid efficiently. As can be observed, the mission can be completed in 765 seconds, which corresponds to the maximum flight time, with flight times as evenly balanced as the power grid configuration allows, even if the flight distances differ as a consequence of the different inspection speeds of the heterogeneous multi-UAV team. Thus, the planner exploits the different inspection speeds to unevenly allocate the power grid, ensuring the mission is completed in the shortest possible time. All UAVs can complete the operation without the need to recharge batteries during the mission execution, as none of the paths exceeds the energy capacity that can be provided by a single battery set. Also, Fig. 14 (bottom) highlights the importance of incorporating terrain elevation into the planning process for

Table 4 Technical specifications of the multi-UAV team

Parameter	*DeltaQuad Pro*	*DJI M210*
Mass	$5kg$	$5.15kg$
Dimensions	$235 \times 90 \times 17cm$	$89 \times 88 \times 41cm$
Max. flight time	$88min$	$41min$
Max. speed	$28m/s$	$23m/s$
Stall speed	$12m/s$	–
Max. wind	$9m/s$	$12m/s$
Max. altitude	$4000m$	$3000m$
Resolution (Flir)	$4000 \times 3000 px$	–
FoV (Flir)	$56 \times 45°$	–
Resolution (X5S)	–	$4096 \times 2160 px$
FoV (X5S)	–	72° (diagonal)
Resolution (XT2)	–	$3840 \times 2160 px$
FoV (XT2)	–	$57.12 \times 42.44°$

The acronym FoV stands for Field of View

Table 5 Planning parameters for the multi-UAV inspection under real-world conditions

Parameter	Value
Inspection velocity (*DeltaQuad Pro*)	$15m/s$
Inspection velocity (*both DJI M210*)	$7m/s$
Distance to power grid (*DeltaQuad Pro*)	$30m$
Distance to power grid (*both DJI M210*)	$10m$
Video perspective (all UAVs)	45°
Temperature[1]	$14.2°C$
Atmospheric pressure[1]	$102100 Pa$
Wind velocity[1]	$4.61m/s$
Wind direction[1]	248°
Battery threshold α used for clustering	0.1

[1]Data automatically acquired from the API for weather estimates

[11] https://www.atlascenter.aero/en/

[12] https://www.deltaquad.com/products/pro/

[13] https://www.dji.com/support/product/matrice-200-series

[14] https://www.raspberrypi.com/products/raspberry-pi-4-model-b/

[15] https://www.skycharge.de/drone-charging-pad

[16] https://www.mathworks.com/help/optim/ug/intlinprog.html

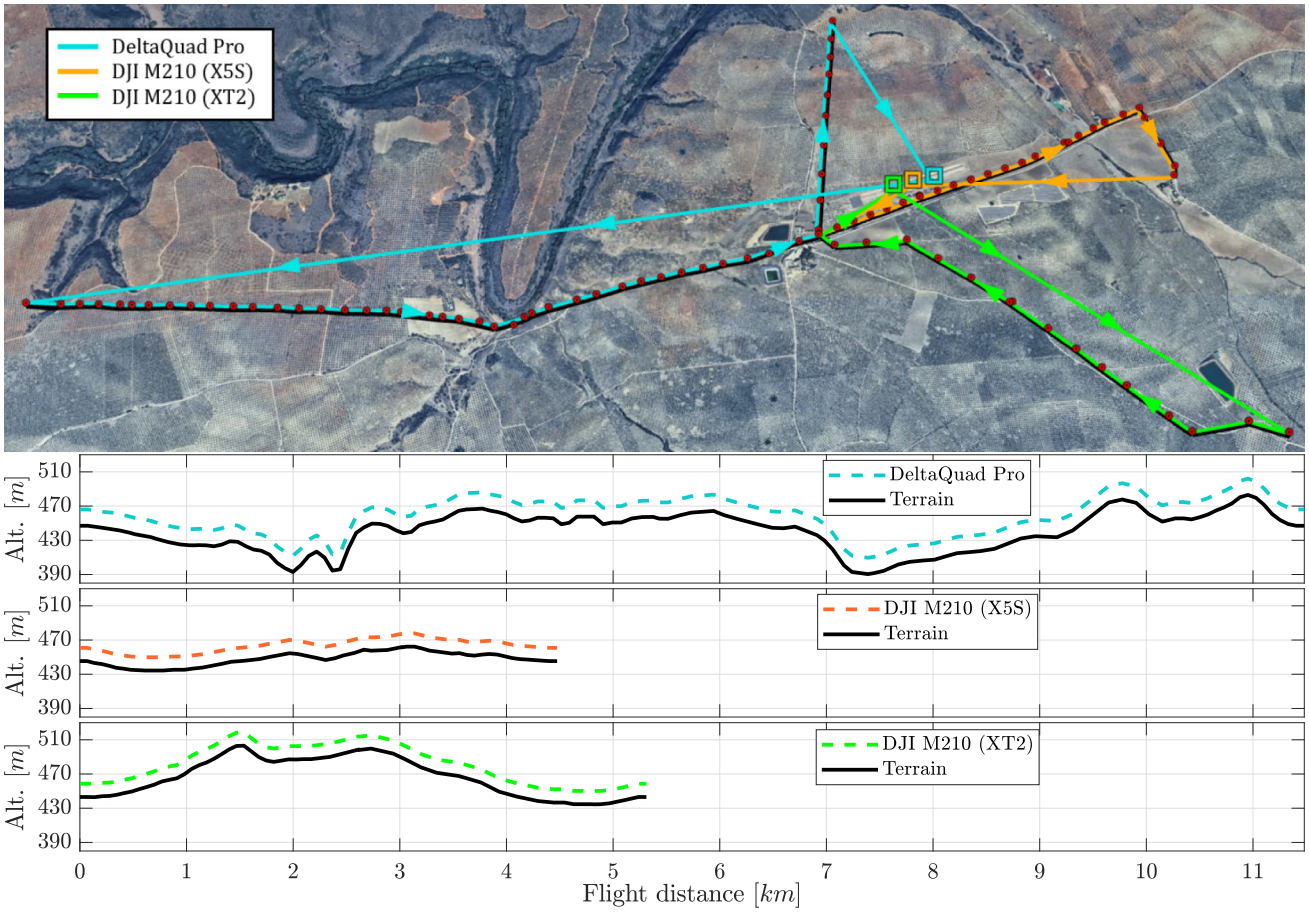

Fig. 14 Paths planned for the multi-UAV inspection under real-world conditions: ground projections (top) and flight altitudes (bottom)

accurate UAV vertical positioning relative to the power line, since it shows significant variations along the paths that may lead to inspection inaccuracies or even UAV crashes if they are not considered.

Once the mission plan was ready, it was automatically exported to a *yaml* file for mission execution and monitoring from the GCS. After approval by the operator, the multi-UAV team autonomously executed the inspection, as illustrated in Fig. 1, while streaming the recorded videos to the GCS. Figure 15 shows two examples with snapshots of the captured videos. Overall, these videos fulfil the Requirements 1-3 in Section 2, since they provide a suitable video perspective, capture all the elements of the power grid and its surroundings, cover the entire length of the power lines, and are georeferenced at all times in order to pinpoint the exact location of any defect that might be found in the power grid. Thanks to these features, the simulated power outage and its exact location were successfully identified (see the bottom side of Fig. 15). The latter reduces costs and enables a fast response to the problem by allowing the subsequent deployment of human operators directly to the target place, having an overview of the fault even before arriving, which helps to prepare a repair plan and the equipment needed in advance. Also, it should be highlighted that the experiment was affected by moderate wind conditions as shown in Fig. 15 (bottom), evidenced by the movement of the piece of plastic

Table 6 Paths planned for the multi-UAV inspection under real-world conditions: main characteristics. The most significant values for each metric have been highlighted in bold

UAV	Flight time	Flight distance	Covered power-grid distance	Batt. consumption
DeltaQuad Pro	**765s**	**11481m**	**5506m**	14.49%
DJI M210 (X5S)	639*s*	4475*m*	2408*m*	25.98%
DJI M210 (XT2)	759*s*	5312*m*	2576*m*	**30.85%**

Fig. 15 Snapshots of the georeferenced videos recorded by the multi-UAV team during the autonomous mission execution under real-world conditions: example of transmission tower (top) and piece of greenhouse plastic sheet hanging from one of the wires connecting two towers and simulating a power outage (bottom)

sheet hanging from the wire. However, this windy conditions did not significantly impact the quality of the results thanks to the stable performance of all the UAVs and the effective video stabilization capabilities of their onboard cameras.

The planning results have also been compared to those obtained using the state-of-the-art approach proposed in [14]. This route planner extends the well-known TSP for the inspection planning of power transmission lines. The method is designed for multi-tour one-depot scenarios and assumes the use of a single UAV, but if the inspection mission exceeds the time that the UAV can fly in one tour, the approach proposes that the multi-tour solution can be distributed between multiple robots to expedite the inspection. Nevertheless, all UAVs are restricted to operate from the same location and must have identical capabilities in terms of inspection speed and battery consumption. Consequently, heterogeneous multi-UAV teams, like the one selected in this paper, cannot be accommodated.

Figure 16 depicts the path planned using the state-of-the-art approach. The path remains the same whether the mission is computed for the multi-rotor or the fixed-wing UAVs. In both cases, the mission can be completed with a single set of batteries, which prevents the planner from proposing the deployment of a multi-UAV team, even with homogeneous capabilities. Moreover, Table 7 summarises the main characteristics of the path when it is planned for the fixed-wing UAV *DeltaQuad Pro* or a multi-rotor UAV *DJI M210*. Although these paths can be computed in less than one second, the table shows longer mission times compared to the one computed in Table 6 with the novel approach formulated in this paper, at the time that the remaining available UAVs are not used in the inspection. In this sense, the novel approach achieves a reduction of 29.81% and 67.21% in the total time that is needed to plan and execute the mission when compared to the single use of the fixed-wing UAV *DeltaQuad Pro* or a multi-rotor UAV *DJI M210*, respectively.

Finally, it is important to emphasise that the state-of-the-art approach [14] does not implement several features introduced in this paper, such as accurate UAV positioning relative to the power grid, path adaptation to ensure an appropriate video perspective, or integration of an accurate battery-consumption model. These features have been identified to be essential for the effective operation in real inspections.

8 Conclusion

This article has presented an integrated solution for the fast inspection of overhead power lines by teams of UAVs. The solution addresses the main aspects that must be faced for an effective field operation and simplifies its use by operators for planning, autonomous execution, and monitoring of the inspection mission. Furthermore, the approach also provides results that meet end-user requirements and enables the exploitation of heterogeneous multi-UAV teams in terms of inspection speed and battery consumption, which helps to maximise the utilisation of available robots. In this context,

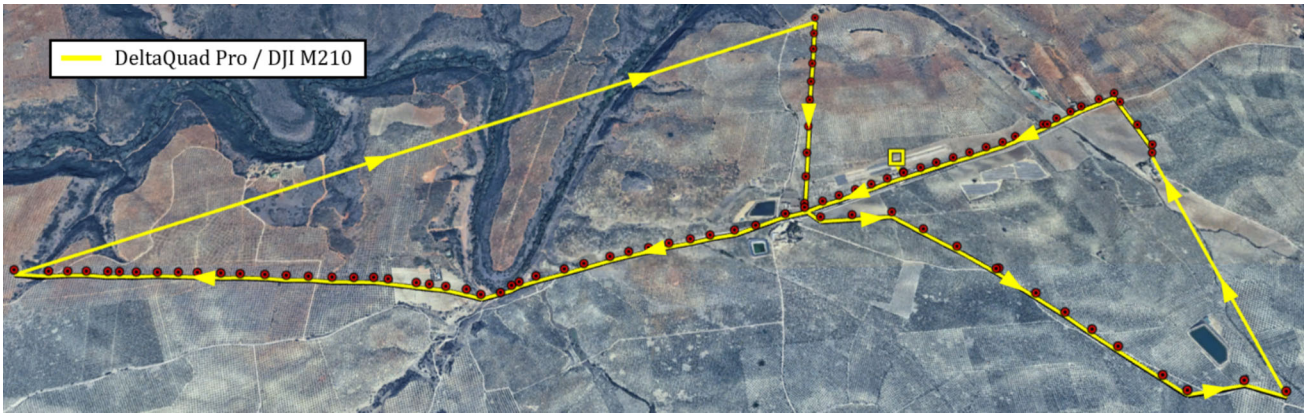

Fig. 16 Path planned using the method described in [14] for the inspection under real-world conditions. The path remains unchanged regardless of whether the mission is executed with the fixed-wing UAV *DeltaQuad Pro* or a multi-rotor UAV *DJI M210*

commercial UAVs with high levels of reliability, robustness, and safety have been combined with custom software specifically designed to address the particularities of the autonomous inspection of overhead power grids, offering a good balance between flexibility and performance. All the aforementioned software has been released as open source, either in this publication or in previous contributions.

The paper has also derived an accurate model of battery consumption, which is used during the planning process to compute feasible routes. The model allows capturing the impact on energy consumption of relevant parameters that are often overlooked, such as UAV mass, inspection speed, or weather conditions, including temperature, atmospheric pressure, and wind magnitude and direction. Comparisons with experimental results have endorsed the validity of the proposed model to estimate real energy consumption accurately, showing relative errors that do not exceed 1.34%.

The integrated solution has been experimentally validated under real-world conditions. Specifically, the inspection of over 10 kilometres of real overhead power lines was planned and autonomously executed in 13 minutes by a heterogeneous multi-UAV team comprising one fixed-wing UAV with VTOL capabilities and two multi-rotor UAVs. This represents a time reduction of up to 67.21% when compared to the state of the art [14]. Finally, the UAV videos streamed during the mission execution proved to be valuable information to detect failures in the power grid and determine their exact locations. Even if the presented solution relied on visual videos, captured with heterogeneous camera models, the sensor-agnostic nature of the formulated planning framework also enables the integration of alternative payloads such as thermal cameras or LiDAR (Light Detection and Ranging) scanners without requiring modification.

Future work includes real-time monitoring of energy consumption on board the UAVs during mission execution to indirectly estimate wind-induced uncertainties and trigger dynamic re-planning whenever deviations may compromise the original plan. It also includes the integration of image-based control loops so that the orientation of the cameras on board the UAVs can be automatically adjusted to keep the power line centred in every frame. Additionally, fault-detection methods based on artificial intelligence can be deployed to automatically highlight anomalies in power lines even under poor contrast, cloudy skies or heavy shadows, eliminating the need for specialised operators to analyse the resulting inspection videos. Finally, machine learning and heuristic/metaheuristic search methods for route planning can also be explored to tackle larger and more complex power grids.

Table 7 Paths planned using the method described in [14] for the inspection under real-world conditions: inspection using the fixed-wing UAV *DeltaQuad Pro* (top) and inspection using a multi-rotor UAV *DJI M210* (bottom)

UAV	Flight time	Flight distance	Covered power-grid distance	Batt. consumption
DeltaQuad Pro	$1116s^{(1)}$	$16733m$	$10490m$	21.14%
DJI M210	$2390s^{(2)}$	$16733m$	$10490m$	97.15%

(1) The approach in this paper achieves a reduction of 29.81% in the total time needed to plan and execute the mission
(2) The approach in this paper achieves a reduction of 67.21% in the total time needed to plan and execute the mission

Acknowledgements The authors would like to thank Victor M. Vega, Miguel Gil and Alvaro R. Poma for their support in conducting the experiments presented in this article, and Jesus Zambrano, as an end user representing the company *e-distribución*, for providing the requirements adopted in this paper for the effective inspection of overhead power lines.

Author Contributions All authors contributed to the study conception and design. Material preparation, data collection and analysis were performed by Alvaro Caballero and Francisco Javier Roman-Escorza. The first draft of the manuscript was written by Alvaro Caballero and all authors commented on previous versions of the manuscript. All authors read and approved the final manuscript.

Funding Funding for open access publishing: Universidad de Sevilla/CBUA. This work has been supported by the European Projects AERIAL-CORE, AEROSUB and SIMAR, funded by the Horizon 2020 and the Horizon Europe research and innovation programmes of the European Commission under grant agreements 871479, 101189723 and 101070604, respectively.

Declarations

Competing Interests The authors have no relevant financial or non-financial interests to disclose.

Code availability The software associated with the planner presented in this article is publicly available in the following *Github* repository: https://github.com/grvc-robotics-lab/multiUAV_planner/ (accessed on 30 November 2024).

Ethics approval Not applicable.

Consent to participate Not applicable.

Consent to publish Not applicable.

Open Access This article is licensed under a Creative Commons Attribution 4.0 International License, which permits use, sharing, adaptation, distribution and reproduction in any medium or format, as long as you give appropriate credit to the original author(s) and the source, provide a link to the Creative Commons licence, and indicate if changes were made. The images or other third party material in this article are included in the article's Creative Commons licence, unless indicated otherwise in a credit line to the material. If material is not included in the article's Creative Commons licence and your intended use is not permitted by statutory regulation or exceeds the permitted use, you will need to obtain permission directly from the copyright holder. To view a copy of this licence, visit http://creativecommons.org/licenses/by/4.0/.

References

1. Küfeoğlu, S., et al.: Economic impacts of electric power outages and evaluation of customer interruption costs. PhD thesis, Aalto University, Helsinki (Finland) (2015)
2. PLP: UAV-installed bird diverters. https://plp.com/energy/distribution/wildlife-protection/uav-installed-bird-diverters. Accessed 30 Nov 2024
3. Paneque, J., Valseca, V., Martínez-de Dios, J., Ollero, A.: Autonomous reactive LiDAR-based mapping for powerline inspection. In: 2022 International Conference on Unmanned Aircraft Systems (ICUAS), pp. 962–971 (2022). IEEE
4. Xing, J., Cioffi, G., Hidalgo-Carrió, J., Scaramuzza, D.: Autonomous power line inspection with drones via perception-aware MPC. In: 2023 IEEE/RSJ International Conference on Intelligent Robots and Systems (IROS), pp. 1086–1093 (2023). IEEE
5. Caballero, A., Silano, G.: A signal temporal logic motion planner for bird diverter installation tasks with multi-robot aerial systems. IEEE Access. **11**, 81361–81377 (2023)
6. Cacace, J., Orozco-Soto, S.M., Suarez, A., Caballero, A., Orsag, M., Bogdan, S., Vasiljevic, G., Ebeid, E., Rodriguez, J.A.A., Ollero, A.: Safe local aerial manipulation for the installation of devices on power lines: AERIAL-CORE first year results and designs. Appl. Sci. **11**(13), 6220 (2021)
7. Iversen, N., Kramberger, A., Schofield, O.B., Ebeid, E.: Pneumatic-mechanical systems in UAVs: autonomous power line sensor unit deployment. In: 2021 IEEE International Conference on Robotics and Automation (ICRA), pp. 548–554 (2021). IEEE
8. Afifi, A., Corsini, G., Sable, Q., Aboudorra, Y., Sidobre, D., Franchi, A.: Physical human-aerial robot interaction and collaboration: exploratory results and lessons learned. In: 2023 International Conference on Unmanned Aircraft Systems (ICUAS), pp. 956–962 (2023). IEEE
9. He, T., Zeng, Y., Hu, Z.: Research of multi-rotor UAVs detailed autonomous inspection technology of transmission lines based on route planning. IEEE Access. **7**, 114955–114965 (2019)
10. Yang, L., Fan, J., Liu, Y., Li, E., Peng, J., Liang, Z.: A review on state-of-the-art power line inspection techniques. IEEE Trans. Instrum. Meas. **69**(12), 9350–9365 (2020)
11. Foudeh, H.A., Luk, P.C.-K., Whidborne, J.F.: An advanced unmanned aerial vehicle (UAV) approach via learning-based control for overhead power line monitoring: A comprehensive review. IEEE Access. **9**, 130410–130433 (2021)
12. Baik, H., Valenzuela, J.: Unmanned aircraft system path planning for visually inspecting electric transmission towers. Journal of Intelligent & Robotic Systems. **95**, 1097–1111 (2019)
13. Silano, G., Baca, T., Penicka, R., Liuzza, D., Saska, M.: Power line inspection tasks with multi-aerial robot systems via signal temporal logic specifications. IEEE Robotics and Automation Letters. **6**(2), 4169–4176 (2021)
14. Nekovar, F., Faigl, J., Saska, M.: Multi-tour set traveling salesman problem in planning power transmission line inspection. IEEE Robot. Autom. Lett. **6**(4), 6196–6203 (2021)
15. Liu, Y., Shi, J., Liu, Z., Huang, J., Zhou, T.: Two-layer routing for high-voltage powerline inspection by cooperated ground vehicle and drone. Energies **12**(7), 1385 (2019)
16. Petitprez, E., Georges, F., Raballand, N., Bertrand, S.: Deployment optimization of a fleet of drones for routine inspection of networks of linear infrastructures. In: 2021 International Conference on Unmanned Aircraft Systems (ICUAS), pp. 303–310 (2021). IEEE
17. Wang, J., Wang, G., Hu, X., Luo, H., Xu, H.: Cooperative transmission tower inspection with a vehicle and a UAV in urban areas. Energies **13**(2), 326 (2020)
18. Li, K., Yan, X., Han, Y.: Multi-mechanism swarm optimization for multi-UAV task assignment and path planning in transmission line inspection under multi-wind field. Appl. Soft Comput. **150**, 111033 (2024)
19. Zhang, H., Ge, H., Yang, J., Tong, Y.: Review of vehicle routing problems: models, classification and solving algorithms. Archives of Computational Methods in Engineering, 1–27 (2021)
20. Hayajneh, M., Al Mahasneh, A.: Guidance, Navigation and Control System for Multi-Robot Network in Monitoring and Inspection Operations. Drones. **6**(11), 332 (2022)

21. Caballero, A., Roman-Escorza, F.J., Maza, I., Ollero, A.: A Multi-UAV Route Planning Method for Fast Inspection of Electric Power Transmission Lines. In: 2024 International Conference on Unmanned Aircraft Systems (ICUAS), pp. 835–842 (2024). IEEE
22. Laporte, G.: The traveling salesman problem: An overview of exact and approximate algorithms. Eur. J. Oper. Res. **59**(2), 231–247 (1992)
23. Costa, J.G.C., Mei, Y., Zhang, M.: Cluster-based hyper-heuristic for large-scale vehicle routing problem. In: 2020 IEEE Congress on Evolutionary Computation (CEC), pp. 1–8 (2020). IEEE
24. Leishman, G.J.: Principles of Helicopter Aerodynamics. Cambridge University Press, Cambridge (2006)
25. Dorling, K., Heinrichs, J., Messier, G.G., Magierowski, S.: Vehicle routing problems for drone delivery. IEEE Transactions on Systems, Man, and Cybernetics: Systems. **47**(1), 70–85 (2016)
26. Bauersfeld, L., Scaramuzza, D.: Range, endurance, and optimal speed estimates for multicopters. IEEE Robotics and Automation Letters. **7**(2), 2953–2960 (2022)
27. Karydis, K., Kumar, V.: Energetics in robotic flight at small scales. Interface focus. **7**(1), 20160088 (2017)
28. Laporte, G.: Generalized subtour elimination constraints and connectivity constraints. Journal of the Operational Research Society. **37**(5), 509–514 (1986)
29. Achuthan, N., Caccetta, L., Hill, S.: A new subtour elimination constraint for the vehicle routing problem. Eur. J. Oper. Res. **91**(3), 573–586 (1996)
30. Laporte, G.: What you should know about the vehicle routing problem. Nav. Res. Logist. **54**(8), 811–819 (2007)
31. Gil-Castilla, M., Caballero, A., Maza, I., Ollero, A.: Integration of Customized Commercial UAVs with Open-Source Tools in a Heterogeneous Multi-UAV System for Power-Lines Inspection. In: 2024 International Conference on Unmanned Aircraft Systems (ICUAS), pp. 1362–1369 (2024). IEEE
32. Poma, A.R., Caballero, A., Maza, I., Ollero, A.: Open-Source Web-Based Ground Control Station for Long-Range Inspection with Multiple UAVs. In: 2024 International Conference on Unmanned Aircraft Systems (ICUAS), pp. 1385–1392 (2024). IEEE
33. Quigley, M., Gerkey, B., Conley, K., Faust, J., Foote, T., Leibs, J., Berger, E., Wheeler, R., Ng, A.: ROS: an open-source Robot Operating System. In: IEEE International Conference on Robotics and Automation Workshop on Open Source Software (2009). IEEE
34. Alejo, D., Conde, R., Cobano, J.A., Ollero, A.: Multi-UAV collision avoidance with separation assurance under uncertainties. In: 2009 IEEE International Conference on Mechatronics, pp. 1–6 (2009). IEEE

Publisher's Note Springer Nature remains neutral with regard to jurisdictional claims in published maps and institutional affiliations.

Alvaro Caballero received the Ph.D. degree in Aerial Robotics from the University of Seville, Spain, in 2022. Since 2014, he has been involved in EU-funded projects such as AEROARMS, HYFLIERS, AERIAL-CORE, OMICRON or AEROSUB. He has also been participating in technology transfer activities in collaboration with leading companies such as Navantia or Endesa. He completed a research stay at the Multi-Robot Systems (MRS) group at the Czech Technical University (CTU) in Prague. He is the author or co-author of more than 20 scientific publications. His main research interests include motion planning for aerial robots in inspection and maintenance.

Francisco Javier Roman-Escorza received the Bachelor's Degree in Electronics, Robotics, and Mechatronics Engineering from the University of Seville and the University of Malaga, with a specialization in Robotics and Automation in 2023. He is currently pursuing an M.Sc. in Robotics at Miguel Hernández University of Elche. Since 2023, he has been with the GRVC Robotics Lab, University of Seville, involved in the AERIAL-CORE and ePark+ projects. His work has been focused on planning for aerial robots and developing simulation tools for inspection and maintenance tasks.

Ivan Maza is Associate Professor at the University of Seville (Spain), received the Telecommunication Engineering Degree in 2000 and joined the GRVC Robotics Lab. He has made research stays at the Automation Technology Laboratory at the Helsinki University of Technology and at the LAAS-CNRS in Toulouse. His Thesis was awarded with the Robotnik Prize to the Best Doctoral Dissertation on Robotics given by the Spanish Committee of Automation in 2010. He authored more than 80 publications on Robotics including more than 30 journal papers indexed in the JCR database and the co-edition of a book published in the Springer STAR Series. His research interests include unmanned aerial vehicles, multi-robot systems, symbolic and motion planning and task allocation techniques. He participated as PI from the University of Seville in the ARCAS Project (2011-2015) devoted to the development and experimental validation of the first cooperative free-flying robot system for assembly and structure construction. In addition, he has participated as co-PI from the University of Seville in the SAFEDRONE Project (2018-2020) funded by EU SESAR JU for the demonstration with drones of U-Space services at the ATLAS flight test center. He has been also PI in several R&D contracts related to different UAV technologies with companies such as Boeing Research and Technology Europe, Navantia and TSK. He has received the "Manuel Losada Villasante Award" in 2021 to excellent researchers in the Innovation category for his work on drone traffic management within the U-space context.

Anibal Ollero is a Full Professor, the Head of the GRVC Robotics Lab, and the Scientific Advisor of the Center for Aerospace Technologies (CATEC) in Seville, Spain. He has authored more than 900 publications. He led more than 190 research projects, participating in more than 41 projects of the European research programs, being coordinator of 7. He has also been recognized with 33 awards, including the Spanish National Research Award in Engineering, the Rei Jaume I in New Technologies, the Overall Information and Communication Technologies Innovation Radar Prize 2017 of the European Commission, and several best paper awards in conferences.